Astron. Astrophys. 346, 1003–1008 (1999)

ASTRONOMY AND ASTROPHYSICS

Non–equilibrium ionization and the interpretation of Yohkoh/SXT data during solar dynamic events

S. Orlando[1], **F. Bocchino**[2], **and G. Peres**[3]

[1] Solar System Division, ESA Space Science Department, ESTEC, Postbus 299, 2200 AG Noordwijk, The Netherlands
[2] Osservatorio Astronomico di Palermo "G.S. Vaiana", Palazzo dei Normanni, I-90134 Palermo, Italy
[3] Dipartimento di Scienze Fisiche ed Astronomiche, sezione di Astronomia, Piazza del Parlamento 1, I-90134 Palermo, Italy

Received 17 February 1999 / Accepted 9 April 1999

Abstract. Yohkoh has been dedicated to study the structure and evolution of the solar corona, especially during dynamic events. During such events, however, the collisional equilibrium ionization – which is invariably assumed when deriving the plasma parameters from the observations – may not apply. We explore the influence of the non–equilibrium ionization effects (NEI) on the values of temperature and emission measure derived from the data collected with the Solar X–ray Telescope (SXT) on board the Yohkoh satellite during solar dynamic events. To this end, we have simulated such dynamic events, assuming that the plasma temperature rises instantaneously from the value T_0 to the value T_1, and then it remains constant. We have considered two different temperature jumps: the first one from $10^{6.3}$ K to $10^{7.3}$ K to simulate a flare and the other, from $10^{5.7}$ K to $10^{6.5}$ K, to simulate a microflare.

We show that the temperature determination with the SXT wide band filter ratio is, to some extent, affected by non–equilibrium ionization: the maximum fractional error on T_1 amounts to ~ 0.7 for the flare and ~ 0.5 for the microflare we have simulated. On the other hand, the emission measure determination can be considerably affected by such departures: the maximum fractional error on EM amounts to ~ 2 for the flare and ~ 7 for the microflare we have simulated. Therefore NEI effects can be important on the temperature and emission measure determination during fast evolving phenomena.

Key words: Sun: activity – Sun: corona – Sun: flares – Sun: X-rays, gamma rays

1. Introduction

The Yohkoh satellite gives us the opportunity to collect solar X–ray data with both high temporal and spatial resolution, and allows us the detailed study of very dynamic events, most notably, solar flares. The Soft X–ray Telescope (SXT; Tsuneta et al. 1991) on board Yohkoh in particular is able to collect images of the solar disk and to discriminate different X–ray spectral bands with filters. The ratio of flux measured in different bands allows the diagnostics of temperature and emission measure, usually determined under the assumptions of plasma isothermality and collisional ionization equilibrium (CIE). The high temporal and spatial resolution jointly with the capability to provide plasma temperature and emission measure diagnostics, make Yohkoh/SXT a powerful and useful instrument to investigate the physical properties of the coronal plasma.

One of the main tasks of Yohkoh (and SXT in particular) has been the study of dynamic, fast evolving, phenomena. During such events, however, CIE conditions may not apply. For instance, during a flare the physical properties of the plasma change very rapidly because of the very rapid increase of temperature. If the timescale of the temperature evolution is much shorter than the ionization and recombination timescale, the degree of ionization can be very different from the equilibrium conditions corresponding to the local electron temperature. In particular, during a fast temperature increase, the plasma ions can be at a lower ionization state than the equilibrium state corresponding to the instantaneous temperature, so the non–equilibrium ionization (NEI) effects may play a non–negligible role in the data interpretation. An equivalent or even larger departure from the equilibrium values may occur as a consequence of a sudden temperature decrease; however the temperature decays of most of all the phenomena observed by Yohkoh are much more gradual than the observed temperature increases, so we will concentrate on the latter.

Yohkoh/SXT data have shown several kinds of dynamic phenomena, ranging from flares lasting several hours, to very fast and impulsive flares; other events, such as microflares, are of low brightness and fast, and affect small parts of an active region (Shimizu & Tsuneta 1997). As a matter of fact the several parts of the solar corona are dynamic with a large range of characteristic evolution times: in this respect ionization conditions out of equilibrium might be rather common in the solar corona.

In the past years, several authors studied in details the behavior of X–ray spectra emitted by plasma under transient conditions typical of solar flares (Kafatos & Tucker 1972; Mewe & Schrijver 1975, 1978, 1980, Sylwester et al. 1980; Mewe & Gronenschild 1981; Mewe et al. 1985). Non equilibrium conditions may affect the plasma diagnostics in various ways, depending on the diagnostic tool and other factors such as instrument inte-

Send offprint requests to: orlando@so.estec.esa.nl

gration time, its spectral resolution, and the spatial and spectral coverage.

Our task is to determine how non equilibrium conditions during solar dynamic events may affect the diagnostics of coronal plasma with Yohkoh/SXT data collected over wide spectral bands in X–ray. In particular, we will focus on the temperature and emission measure determination of the soft X–ray emitting plasma with the filter ratio method, i.e. the ratio of flux measured through two or more X–ray spectral bands selected with appropriate filters, to diagnose the plasma conditions (Vaiana et al. 1973, Gerassimenko & Nolte 1978, Hara et al. 1992).

This study is motivated by the importance of the SXT data set in solar physics and the standard use of the filter ratio method as a diagnostic tool. We will simulate two cases which represents an example of two solar dynamic events: a flare heating and a microflare heating. Comparing the results obtained with the standard filter ratio method on simulated results and the "real" input temperature and emission measure, we will be able to evaluate biases introduced into the standard analysis by neglecting the NEI effects.

The paper is structured as follows: in Sect. 2 we describe the method of analysis adopted to investigate the NEI effects during dynamic events; in Sect. 3 we present the results obtained in the case of a flare and a microflare; and in Sect. 4 we draw our conclusions.

2. Method of analysis of NEI effects

To evaluate the NEI effects on Yohkoh/SXT diagnostics of solar dynamic events, we used a model which allows us to concentrate on the NEI effects. We assumed that before the heating occurring at time t_0 the plasma is at temperature T_0 and is in CIE. At t_0, its temperature rises instantaneously to $T_1 > T_0$ and then it remains constant: we have considered the most drastic case of a temperature rise time negligible with respect to every other plasma time scale involved. This evolution leads to a NEI condition and the system evolves toward a CIE situation at the new temperature T_1, achieved approximately after a time $t_{\rm CIE}$ after t_0.

If a Yohkoh/SXT observation is made between t_0 and $t_0 + t_{\rm CIE}$, and the temperature is evaluated assuming CIE conditions, an error can be made in principle. However, since the temperature is evaluated on the basis of the ratios between emission over broad bands and the comparison with calibration curves, computed assuming CIE, it is not immediate to predict the deviation of the Yohkoh estimated temperature from the real temperature T_1 vs. the time since the onset of the perturbation.

We have chosen to investigate two different physical situations: a flare, and a microflare as observed by SXT on board Yohkoh. The first is an instantaneous jump of temperature from $10^{6.3}$ K to $10^{7.3}$ K, the second is an analogously instantaneous jump of temperature from $10^{5.7}$ K to $10^{6.5}$ K. For each case, we calculated NEI spectra between t_0 and $t_0 + t_{\rm CIE}$, and we evaluated the coronal spectra folded through the Yohkoh/SXT total spectral response with various filters. Then, we derived the temperature of the plasma using the Standard Yohkoh Analysis Software (in the following SYAS), and we compared it with the input electron temperature, T_1. This model allows us to isolate and study the effects of the ionization conditions gradually reaching equilibrium after a temperature jump without additional complications.

2.1. NEI computations of the X–ray synthetic spectra

In order to compute the NEI emission of the plasma between t_0 and $t_0 + t_{\rm CIE}$, we have first calculated the population fraction versus time, and then the spectrum at selected times.

To compute the population fraction, we solved, for the set of 12 most abundant heavy elements (He, C, N, O, Ne, Mg, Si, S, Ar, Ca, Fe, Ni), the set of NEI equations, as given for instance by Masai (1994), keeping the temperature, T, and the electron number density, N_e, constant in time:

$$\frac{\partial n_i}{\partial t} = N_e \left[\alpha_{i+1} n_{i+1} + S_{i-1} n_{i-1} - n_i \left(\alpha_i + S_i\right)\right] \qquad (i = 1, ..., l) \tag{1}$$

where n_i is the number density of ion i, t is the time, and α_i and S_i are, respectively, the recombination and ionization coefficients of ion i with $\alpha_1 = S_0 = \alpha_{l+1} = S_l = 0$. Under this condition, the resulting spectra are identified by two parameters, namely the temperature and the ionization time $\tau = N_e t$, where t is the time elapsed since t_0. The adopted numerical scheme is a fifth order Runge–Kutta method with adaptive stepsize control (by step–doubling; see Press et al. 1986), already used by Bocchino et al. (1997) to build a grid of emission models to be used in fitting of ROSAT/PSPC X–ray data, and by Spadaro et al. (1995) and Orlando & Peres (1999) to analyze the NEI effects caused by siphon flows confined in coronal loops. We assumed that the plasma is initially in conditions of ionization equilibrium at $T = T_0$; therefore the initial value of the density of ion i is obtained from the equations

$$(n_i)_{eq} S_i = (n_{i+1})_{eq} \alpha_{i+1} \qquad (i = 1, ..., l-1) \tag{2}$$

$$\sum_{i=1}^{l} (n_i)_{eq} = A_{el} n_p \tag{3}$$

where n_p is the number density of protons and A_{el} is the abundance of the element relative to the hydrogen. The dependence of the ionization and recombination coefficients on temperature and density have been taken into account following Summers (1974) and Raymond & Smith (1977). This method is more accurate than the Lotz (1967) formula, especially in the case of under ionized NEI plasma, as discussed by Hamilton et al. (1983). In both the flare and microflare cases, we have chosen to sample the ionization population fraction at 50 values of τ ranging between 10^7 and 3×10^{13} s cm^{-3}; the case $\tau > 10^{13}$ s cm^{-3} corresponds, in practice, to CIE conditions (Bocchino et al. 1997).

For each value of τ, we computed the NEI spectrum in both the flare and microflare cases using the Raymond & Smith (1977) emission model and recent updates, as

$$N_\gamma(i,T) = \mathrm{EM}(T) \int dE\ P(T,E)/E \qquad (4)$$

where $N_\gamma(i,T)$ is the number of photons in the i–th energy bin, EM is the emission measure, E is the photon energy, $P(T,E)$ is the spectrum emitted by an optically thin isothermal plasma, and the integral is computed over the energy range of the i–th bin. Emissivity, in units of cnt s^{-1} cm^{-2} bin^{-1}, has been evaluated in 290 energy bins from 2 Å to 110 Å, to sample adequately the Yohkoh/SXT total bandwidth.

2.2. X–ray spectra folded through the Yohkoh/SXT filters

We then simulated Yohkoh/SXT observations from the X–ray synthetic spectra $N_\gamma(i,T)$ computed as above. The SXT instrument is a glancing incidence telescope which forms X–ray wide–band photometric images of the solar corona on a front–illuminated, virtual phase charge coupled (CCD) detector (Tsuneta et al., 1991).

Yohkoh/SXT has six thin metallic filters which allow the observer to separate different X–ray energy bands for plasma temperature diagnostics. In order to analyze the NEI effects on this diagnostics, we have computed $S_{\rm filter}(i,T)$, namely the X–ray emission in each of the spectral bands of interest, by folding the synthetic spectra with the instrumental gain and the SXT filter response functions,

$$S_{\rm filter}(i,T) = \frac{t_{\rm exp}}{4\pi D^2} N_\gamma(i,T) A_{\rm eff}(i)\ , \quad (i=1,...,k) \qquad (5)$$

where i is the label of the energy bins, k is the total number of energy bins, $D(=1$ AU) is the distance to the Sun, $t_{\rm exp}$ is the exposure time, and $A_{\rm eff}(i)$ is the effective area over the band of interest.

From $S_{\rm filter}(i,T)$, we computed the number of electrons $N(e^-)$ produced by the X–ray photons in the CCD, and finally the Data Number (in the following DN), i.e. the final output emerging from the analogue to digital converters of Yohkoh/SXT (Tsuneta et al. 1991).

2.3. Determination of the temperature and emission measure

The different SXT analysis filters provide the observer with a wide–band spectral resolution. Almost simultaneous observations (usually within 2 s when SXT is operating in *flare mode*) through different filters allow the observer to determine the temperature of the emitted plasma on the basis of the ratio between flux collected in the chosen bands, on the basis of calibration curves (Hara et al. 1992). The emission measure of the emitted plasma can be derived from the flux collected through one of the two filters, using the estimated temperature and the filtered coronal spectrum. CIE conditions are always assumed.

We have derived the temperature and emission measure from the flux ratio measured by Yohkoh/SXT from the observations of the plasma as its spectrum evolves in time after the temperature jump. The scope is to ascertain how much the temperature and emission measure values, as determined with the Standard Yohkoh data Analysis, differ from the real values.

We derived the temperature of the plasma from our simulated DN values obtained both in the flare and the microflare cases, using the SYAS. Since we synthesized the X–ray spectra using the updated version of the Raymond & Smith (1977) spectral code, we used it also to produce the calibration curves to derive temperature and emission measure within the SYAS instead of the theoretical X–ray spectra of Mewe et al. (1985, 1986) commonly used.

3. Results and discussion

We have assumed a plasma density of $N_e = 10^{10}$ cm^{-3} for both our simulations and we have represented the flare as a sudden increase from $T_0 = 10^{6.3}$ K to $T_1 = 10^{7.3}$ K, i.e. from a normal corona to a flaring corona, while the microflare is modeled as a sudden increase from $T_0 = 10^{5.7}$ K to $T_1 = 10^{6.5}$ K, i.e. heating plasma to coronal conditions.

The DN values are proportional to $t_{\rm exp} \times$ EM. In deriving the folded spectrum, we assumed for both cases a product $t_{exp} \times \mathrm{EM} = 10^{48}$ s cm^{-3}, amounting to an emission measure of the plasma EM $= 10^{50}$ cm^{-3} which is typical of solar flare conditions, and an exposure time $t_{\rm exp} = 10$ ms which is of the order of magnitude of standard exposure times of Yohkoh/SXT during a flare. To simulate the observation of a flare, we selected the 1265 Å Al filter (referred to as Al.1) and the composite filter, made of 2930 Å Al, 2070 Å Mg, 562 Å Mn, and 190 Å C (referred to as AlMg), and that of the 11.6 μm Al (Al12) and the 119 μm Be (Be119) filters, the latter pair of filters being the most appropriate to observe plasma with temperatures from $10^{6.7}$ K to a few 10^7 K and usually selected to observe flares. In the microflare case, we selected the pair of Al.1 and AlMg filters, because they are more appropriate to observe plasma at temperature ranging from 10^6 K to 10^7 K. The results describe the consequences of the evolution of the spectrum, as the plasma gradually reaches CIE, on the band–ratio values and on the results of temperature and emission measure determination with SYAS.

A fundamental hypothesis of our study is that the temperature variations occur in a time scale shorter than other plasma time scales. In particular, we have calculated the electron thermalization time τ_e according to Spitzer (1962) and, in the cases examined, we have found $\tau_e \sim 0.1$ s for the flare and $\tau_e \sim 0.01$ s for the microflare. Since the spectra change over a time scale larger by orders of magnitude our hypothesis is realistic.

In Fig. 1, we show the plasma temperature (thick line) vs. $\log t$, the time elapsed since the onset of the flare, and the corresponding emission measure values (thin line) derived from the pair of filters Al12 and Be119 with the SYAS under the CIE assumption. We provide the time in seconds assuming a density of $N_e = 10^{10}$ cm^{-3}. Since the ionization calculations depend on the product $N_e t$, it is easy to evaluate the corresponding results for higher, or lower, density values. As expected the de-

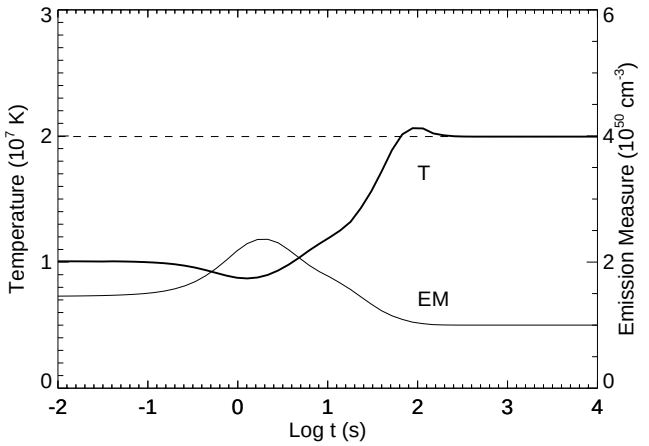

Fig. 1. Plasma temperature (thick line) and emission measure (thin line) determined with the standard Yohkoh analysis software under CIE assumption vs. the logarithm of the time elapsed since the onset of the temperature jump from $10^{6.3}$ K to $10^{7.3}$ K. The dashed horizontal line marks the final value of the temperature T_1. We have assumed to use the 11.6 μm Al (Al12) and the 119 μm Be (Be119) filters. We have also assumed an electron number density of 10^{10} cm^{-3}. Since the results depend on the product of the density and the elapsed time, they can be used for other density values by changing the time scale.

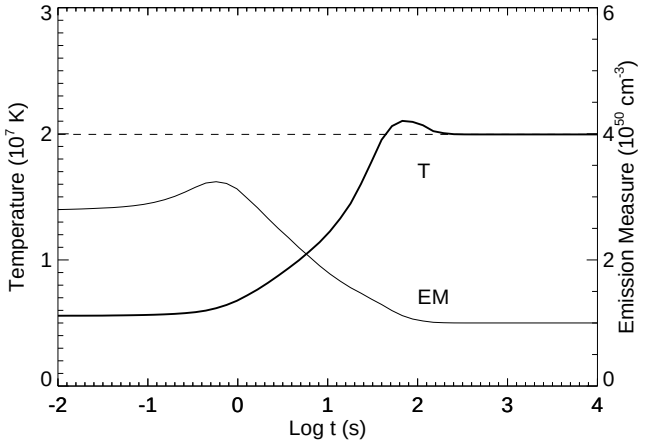

Fig. 2. As in Fig. 1, assuming to use the 1265 Å Al filter (Al.1), and the composite filter comprising 2930 Å Al, 2070 Å Mg, 562 Å Mn, and 190 Å C (AlMg).

rived temperature and emission measure asymptotically reach the T_1 (dashed line in the figure) and EM values (specifically for $t > 10^2$ s), but significant discrepancies exist at lower t. In Fig. 2, we show the analogous results using the pair of filters Al.1 and AlMg. The differences with the previous case are remarkable for $t < 10$ s, where the temperature values derived are significantly lower (and the emission measure values higher) than those derived with the Al12–Be119 pair.

The analysis of the folded X–ray spectra is useful to understand the evolution of the derived thermodynamic parameters discussed above. In Figs. 3 and 4 we report the spectra folded through the four SXT filter response functions used in our analysis, at three different times. These figures point out that the contribution of the continuum to the spectrum does not change much from $\log t = -3$ to $\log t = 4$, showing how quickly it follows the variation in the electron temperature already in the early phase of the evolution. On the other hand, the contribution of the emission lines only gradually adapts itself to the sudden change of the ambient temperature and it is mostly responsible for the delay in reaching the asymptotic values. Since the line contribution is larger at longer wavelengths, the changes in the spectrum are much more significant at longer wavelengths than at shorter wavelengths.

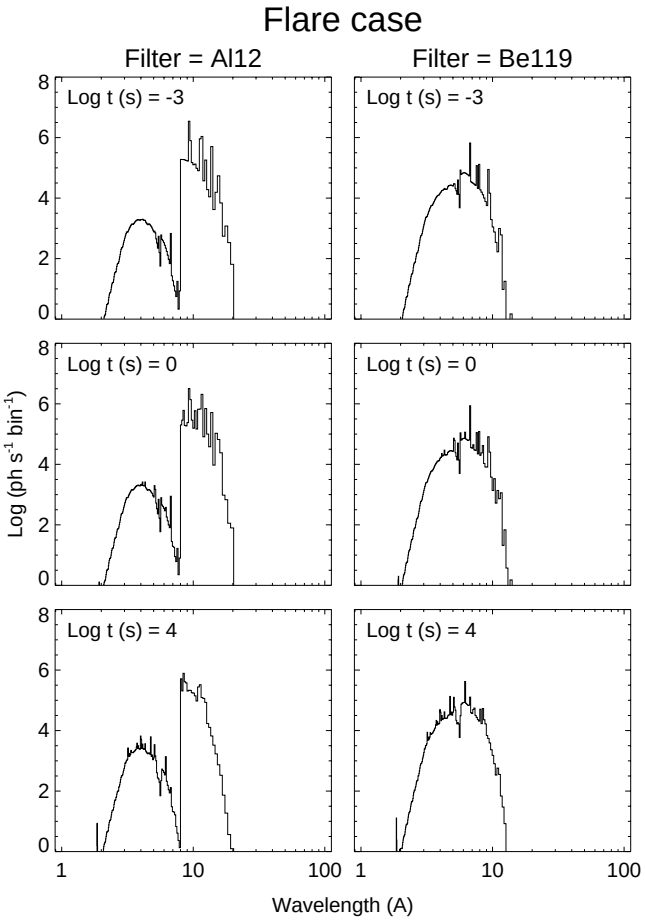

Fig. 3. Emitted spectrum during the flare folded through the Al12 (on the left) and Be119 (on the right) filter response functions. We show three different times during the evolution, namely $\log t(\mathrm{s}) = -3, 0, 4$.

On the basis of these considerations, it is easy to explain the evolution of the temperature and emission measure values derived with SYAS. The filters Al12 and Be119 are both hard filters so that they cover an energy band in which the contribution of the continuum is much more important than the contribution of the emission lines. Therefore, the derived temperature is closer to (but still significantly different from) the final value even at the early stage of the evolution. This is not the case for the other pair of filters, namely Al.1 and AlMg. In this case, in fact, the energy band covered is softer than the one in the previous case and the contribution of the emission lines is very important. As a consequence, the temperature derived during the first phase of the evolution ($T \sim 5.5 \times 10^6$ K) is considerably lower than the final one ($T_1 \sim 2 \times 10^7$ K), much closer to the temperature

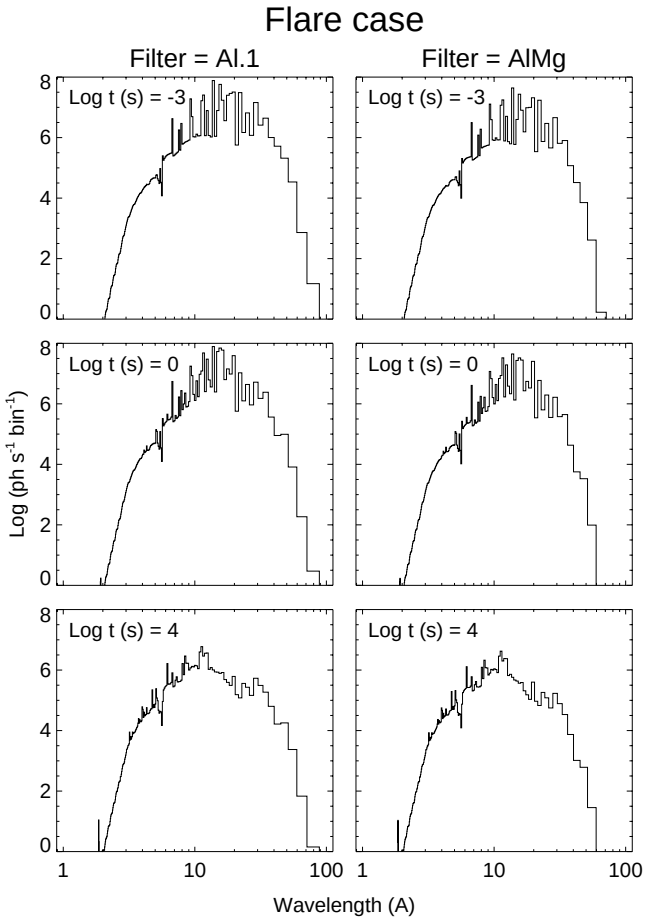

Fig. 4. As in Fig. 3, for the Al.1 (on the right) and AlMg (on the left) filters.

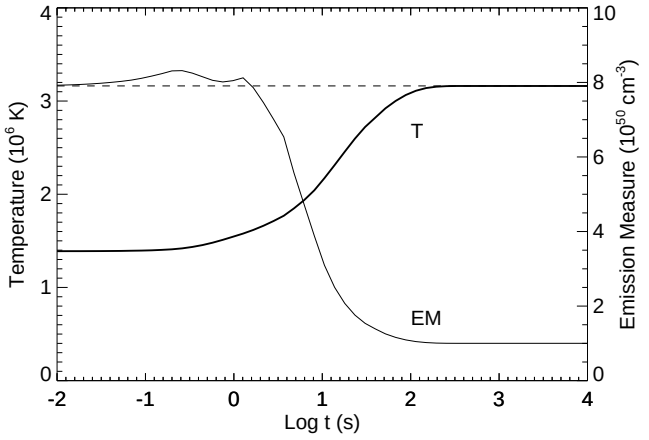

Fig. 5. The same as Fig. 1 but for the "microflare" case; also in this case we have assumed an electron number density of 10^{10} cm^{-3}. Here we have assumed to use the Al.1 and AlMg filters.

before the onset of the flare ($T_0 \sim 2 \times 10^6$ K) and definitely lower than that derived with the pair of hard filters ($T \sim 10^7$ K).

Analogously to Figs. 1 and 2, in Fig. 5 we show the evolution of the derived plasma temperature and emission measure for the microflare heating using the pair of filters Al.1 and AlMg. As in the previous case, the derived temperature asymptotically

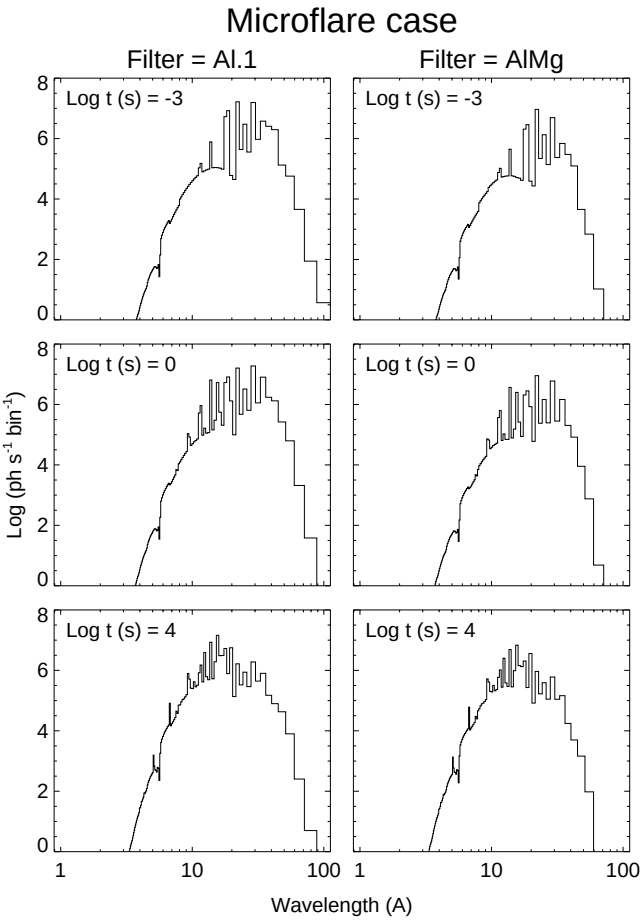

Fig. 6. As in Fig. 3 for the "microflare" case, and assuming to use the Al.1 (on the left) and AlMg (on the right) filters.

reaches the T_1 value for $t > 10^2$ s, but now the derived T and EM for $t < 10^2$ s are very close to the input values. Fig. 6 shows the spectra folded through Al.1 and AlMg filters for three different times during the evolution of the microflare. The major change in the spectra is again at long wavelengths where the contribution of the emission lines is important. These characteristics are reflected in the moderate variations during the evolution of the inferred temperature. On the other hand, significant discrepancies on emission measure exist at lower t (< 10 s) where the fractional error reaches ~ 7.

4. Conclusions

Our results show that the temperature determination with the Yohkoh/SXT wide band filter ratio can be affected by departures from CIE. The results may depend on the set of filters used and, for the flare case, we have found that the hardest filters yield results closer to the asymptotic CIE values because of the more preeminent continuum contribution. In fact the continuum quickly follows the variation of the ambient temperature reaching the new equilibrium condition already in the early phase of the evolution. As a consequence, the larger the contribution of the continuum to the observed part of the spectrum, the closer to the asymptotic temperature T_1 is the derived temperature.

This effect explains the differences between the values derived with two different pair of filters that we have found in the analysis of the flare case. Even in the early phase of the evolution, the temperature derived with the "hard" pair of filters, namely Al12 and Be119, is closer to the input value T_1 than that derived with the "soft" pair of filters Al.1 and AlMg. The reason is that such pairs of filters cover different energy bands and the contribution of the continuum to the flux in the band is more important for the first pair than for the second. Note that the "hard" pair of filters is commonly used for the observation and analysis of flares.

It is worth noting that the differences between the plasma characteristics derived in our simulations with the two pair of filters are entirely due to the non–equilibrium ionization effects on the emission lines and, therefore, this effect can be used, in principle, as a way to check the validity of the CIE assumption in the data analysis. On the other hand it is to be noted that when observing a multi–temperature plasma within each pixel, which can be the case, different temperature values with different filter pairs can be measured, even if the plasma is in CIE conditions. Another possible signature that an observer could look for to see whether departure from equilibrium is important is suggested in Figs. 1 and 2 where the overestimate of the emission measure in comparison to the "real" modeled value, EM $= 10^{50}$ cm^{-3}, is apparent. If we consider the conditions before the onset of the flare ($T \sim 2 \times 10^6$ K and EM $= 10^{50}$ cm^{-3} at $t \leq t_0$), the interpretation of the filter ratios with the standard Yohkoh CIE curves would show a long period of constant temperature and emission measure (for $t \leq t_0$) and a brief period ($\sim$ 1–10 s since the onset of the flare, see Figs. 1 and 2) at the same or somewhat higher temperature and considerably higher emission measure, followed by a period (after 100 s since the onset of the flare) of constant high temperature and low emission measure. This is obviously far from foolproof and the interpretation of real observations is considerably complicated by the fact that real emission measure may increase due to evaporation, compression or heating of really cold gas.

The discrepancy between the "input" and the derived values of the emission measure can be large for $t < 10$ s in both the cases examined. In particular, in the flare analysis the emission measure can be overestimated by a factor 1.5–2 around $t \sim 1$ s using the "hard" pair of filters Al12 and Be119 (see Fig. 1), and even by a factor 3 using the "soft" pair of filters Al.1 and AlMg (Fig. 2). Concerning the microflare analysis, the discrepancies may be even larger than in the flare case and the emission measure may be overestimated by a factor 8 (Fig. 5).

Our analysis points out that the influence of NEI effects on the temperature interpretation of SXT data during solar dynamic events are not negligible and that the emission measure analysis may be strongly affected by departures from CIE as discussed above. An additional complication to the interpretation comes from the fact that the minimum time between two consecutive real Yohkoh/SXT exposures is $\sim$ 2 s and Figs. 1, 2 and 5 show that within this time the extent of the NEI effects and plasma conditions may be very different. This means that, if accurate measurements are needed for relatively fast evolving plasmas, proper account of the NEI effects can be crucial.

It is worth pointing out that other effects may significantly affect the temperature and emission measure interpretation of the Yohkoh/SXT data and they should be taken into account. For instance, Li et al. (1998) have found that different sets of elemental abundances have visible effects on the temperature and emission measure derived from Yohkoh/SXT data.

Our analysis shows that, albeit NEI effects are very evident, the wide bands used for Yohkoh/SXT observations somehow mitigate the errors due to the assumption of CIE while the plasma emission is not in equilibrium conditions, mostly because of the large continuum contribution and because several lines are observed simultaneously. However our analysis also suggests, that NEI effects may be much more important for observations over narrow bands (like those observed, for instance, by TRACE) and, a fortiori, when observing isolated spectral lines. The relevant studies may be the subject of future papers.

Acknowledgements. We wish to thank the referee, Dr. J. Raymond, for his useful criticisms and suggestions to the paper. FB and GP acknowledge partial support from the Ministero della Università Ricerca Scientifica e Tecnologica and the Agenzia Spaziale Italiana. This work was originally inspired by a discussion of S. Tsuneta with GP.

References

Bocchino F., Maggio A., Sciortino S., 1997, ApJ 481, 872
Gerassimenko M., Nolte J., 1978, Solar Phys. 60, 299
Hamilton A.J.S., Sarazin C.L., Chevalier R.A., 1983, ApJS 51, 115
Hara H., Tsuneta S., Lemen J., Acton L., McTiernan J., 1992, PASJ 44, L135
Kafatos M.C., Tucker W.H., 1972, ApJ 175, 837
Li J., Raymond J.C., Acton L.W., et al., 1998, ApJ 506, 431
Lotz W., 1967, ApJS 14, 207
Masai K., 1994, ApJ 437, 770
Mewe R., Gronenschild E.H.B.M., 1981, A&AS 45, 11
Mewe R., Gronenschild E.H.B.M., van den Oord G.H.J., 1985, A&AS 62, 197
Mewe R., Lemen J.R., Peres G., Schrijver J., Serio S., 1985, A&A 152, 229
Mewe R., Lemen J.R., van den Oord G.H.J., 1986, A&AS 63, 511
Mewe R., Schrijver J., 1975, Ap&SS 38, 345
Mewe R., Schrijver J., 1978, A&A 65, 115
Mewe R., Schrijver J., 1980, A&A 87, 261
Orlando S., Peres G., 1999, Physics and Chemistry of the Earth. Proc. of the 23rd EGS General Assembly, Nice (France), 20–24 April 1998
Press W.H., Flannery B.P., Teukolsky S.A., Vetterling W.T., 1986, Numerical Recipes. Cambridge University Press, Cambridge
Raymond J.C., Smith B.W., 1977, ApJS 35, 419
Shimizu T., Tsuneta S., 1997, ApJ 486, 1045
Spadaro D., Orlando S., Peres G., Leto P., 1995, A&A 302, 285
Spitzer L., 1962, Physics of fully ionized gases. Interscience tracts of physics and astronomy
Summers H.P., 1974, Culham Laboratory Internal Memo IM–367, Culham Laboratory, Ditton Park, Slough, England
Sylwester J., Mewe R., Schrijver J., 1980, A&AS 40, 335
Tsuneta S., Acton L., Bruner M., et al., 1991, Solar Phys. 136, 37
Vaiana G.S., Krieger A., Timothy A., 1973, Solar Phys. 32, 81